RSC Advances

PAPER

View Article Online
View Journal | View Issue

Cite this: *RSC Adv.*, 2020, **10**, 7661

Half-metallicity in new Heusler alloys Mn_2ScZ (Z = Si, Ge, Sn)

Mahesh Ram, [ab] Atul Saxena,[a] Abeer E. Aly *[c] and Amit Shankar [b]

Received 9th November 2019
Accepted 13th February 2020

DOI: 10.1039/c9ra09303f

rsc.li/rsc-advances

Study of half-metallicity has been performed in a new series of Mn_2ScZ (Z = Si, Ge and Sn) full Heusler alloys using density functional theory with the calculation and implementation of a Hubbard correction term (*U*). Volume optimization in magnetic and non-magnetic phases for both the Cu_2MnAl and Hg_2CuTi type structures was done to predict the stable ground state configuration. The stability was determined by calculating their formation energy as well as from elastic constants under ambient conditions. A half-metal is predicted for Mn_2ScSi and Mn_2ScGe with a narrow band gap in the minority spin whereas Mn_2ScSn shows a metallic nature. The magnetic moments of Mn and Sc are coupled in opposite directions with different strengths indicating that the ferrimagnetic order and the total magnetic moment per formula unit for half-metals follows the Slater Pauling rule. And a strong effect was shown by the size of the Z element in the electronic and magnetic properties.

1. Introduction

The current pursuit in the field of materials research is to develop a material for spintronics applications, where the spin degree of freedom of an electron plays a significant role in encoding, faster transfer and processing of data as compared to a charged based equivalent transistor,[1,2] as well as low power consumption,[3] high circuit density[4] and non-volatility.[5] The performance of a spintronic device depends on efficiency of spin injection from electrodes to semiconductors and their degree of spin polarization. The spintronic devices mostly consist of a non-magnetic layer sandwiched between two ferromagnetic electrodes like giant-magnetoresistance (GMR),[6,7] tunnelling magnetoresistance (TMJ)[8] and magnetic tunnel junction (MTJ)[9] devices. Half-metallic ferromagnets (HMF) are becoming prominent in this context because of their peculiar electronic structure at the Fermi energy level (E_F), with 100% electron spin polarization.[10,11]

The systems like oxides, manganites, pyrites and double perovskites belongs to HMF,[12–14] but the Heusler alloys are gaining preferences over them due to their stable half-metallicity with high Curie temperature (T_C) (1520 K for Cr_2CoZa,[15] 1100 K for Co_2FeSi[16]) and compatible lattice structure to construct a hetero structure with conventional semiconductor for spintronic devices. The other interesting feature of Heusler alloys is the predictability of their physical properties by simple empirical relation such as Slater-Pauling (SP) rule or by simply knowing the valence electron count, atomic ordering in the lattice, degree of atomic disorder and the strength of exchange interactions.[17,18] The diverse applicability of these Heusler alloys also increases as one can easily tune their electronic and magnetic properties by doping.[19–21]

In previous reports, researchers have predicted half-metallicity in Fe_2YSi (Y = Cr, Mn, Fe, Co and Ni), Ti_2YAl and $Ti_2Y'Ga$ (Y = Co, Fe and Y′ = Cr, Fe) from the theoretical and experimental studies.[22–25] The recent development on the experimental studies of HM in thin film structures of Heusler alloys Co_2MnSi, Co_2FeAl, Fe_2CoSi, Cr_2CoGa, Co_2MnGe and Fe_2CrGa[26–31] also highlights some novel properties such as perpendicular magnetic anisotropy (PMA) as their intrinsic properties which is a requirement for spin transfer torque-random access memory and for skyrmions-based research.

Among the Heusler alloys, Mn_2YZ based members (Y being a 3d or 4d transition element and Z an sp element) are of significant interest due to the presence of Mn^{3+} ion with d^4 electronic configuration that leads to Jahn–Teller tetragonal distortion with partially filled degenerate orbitals.[32,33] The interaction of the long range strain due to Jahn–Teller distortion with magnetic degrees of freedom gives way to multifunctional properties such as exchange bias, magnetocaloric effect and magnetic shape memory alloys.[34–36] Moreover the parallel or antiparallel alignment of two Mn magnetic moments depending on interaction with the neighbouring atoms results in ferromagnetic or ferrimagnetic ordering, respectively.[37,38] Mn_2YZ in ferrimagnetic structure are of more interest due to anti-parallel alignment of two Mn magnetic moments that results in low saturation magnetization reducing the stray fields which makes the devices more resistant to external fields. This

[a]*Department of Physics, North-Eastern Hill University, Shillong, India-793022*
[b]*Condensed Matter Theory Research Lab, Department of Physics, Kurseong College, Kurseong, Darjeeling, India – 734203. E-mail: amitshan2009@gmail.com*
[c]*Basic Science Department, El Salam Institute for Engineering and Technology, Cairo, Egypt. E-mail: abeerresmat782000@yahoo.com*

along with large PMA, high electron-spin polarization with high Tc[39,40] and efficient spin-transfer torque[41] are responsible for making Mn_2YZ Heusler alloys a promising material in future spintronic devices.

Among the Mn_2YZ compounds, Mn_2VAl is the first half-metallic ferrimagnet (HMFi) that was studied both theoretically and experimentally[42,43] followed by Mn_2YZ (Y = V, Cr, Cu, Fe, Co, Ni and Z = Al, Ga, Si, Ge, Sb, Sn)[44–47] Heusler alloys. In this context Wollmann and co-workers[48,49] have reported a tetragonal distortion with reduced electron spin polarization in series of Mn_2YZ, with Y belonging to 3d, 4d and 5d transition elements. Also, among X_2YZ Heusler alloys there exist limited studies predicting half-metal with Y = Sc based materials such as V_2ScP, Cr_2ScAl and $Fe_2ScP/As/Sb$.[50,51] Likewise, to the best of our knowledge, half-metallic properties in Mn_2ScZ (Z = sp elements) Heusler compounds has not been reported so far using experimental or trending density functional theory (DFT). The inefficiency of DFT based conventional exchange correlation functional such as generalized gradient approximation (GGA) and local spin density approximation (LSDA) to predict ground state properties and understand the underlying physics of the strongly correlated d and f transition metals based systems limits to unfold their HM properties.[52] Similar anomaly was also observed in Mott insulators where DFT interpreted metallic bands due to ignorance of the effect of localized d and f orbitals[53–55] resulting in a self-interaction error.[55] This effect is also visible in narrow band oxides[56,57] and molecular systems.[58] The introduction of on-site Coulomb repulsion term (U) in the Hubbard model (DFT+U)[55] corrects the self interaction and consider the effects of localized electrons and removes the inconsistency observed in first principle calculations and experimental results of strongly correlated systems. Heusler alloys are no exception to the inadequacy of DFT and Co_2FeSi is a prototype where the experimental findings could be reproduced theoretically only with the inclusion of U.[59,60] Bandyopadhyay and Sarma[61] have calculated the U values for 3d transition and 5f actinide elements and showed its dependence on the number of electrons. U values for 3d electrons have been calculated experimentally as well.[62,63] At present there are large number of studies in case of Heusler alloys in which calculation of U value and its effect on the electronic and magnetic properties are reported.[64–66] A clear implication of U calculation and its influence on Heusler alloys to predict exact ground state properties can be found from the studies carried out by Rai *et al.*[67,68]

The effect of electron correlation in Heusler alloys are evident from the above literature and it is expected to have significant impact on alloys where highly localized d orbitals based transition metals Mn and Sc are present whose exact ground state properties are yet unexplored. Hence, in view of importance of DFT+U calculation in the material research, an effort have been made to investigate the half metallic behaviour of highly localized Mn and Sc based sample alloys Mn_2ScZ (Z = Si, Ge and Sn) by adding U correction for 3d electrons of Mn and Sc. Their stability at ground state fcc phases were verified by calculating formation energy and their mechanical properties are also estimated using elastic constants at ambient condition.

2. Computational method

We have employed a plane wave pseudopotential (PW-PP)[69] and full potential-linearized augmented plane wave (FP-LAPW)[70] methods based on density functional theory for the study presented in this manuscript. In FP-LAPW method, the space is divided into a non-overlapping muffin-tin (MT) spheres centred on the atomic sites and in an interstitial region. Inside the MT spheres, the basis set is consist of a linear combination of product of radial functions and the spherical harmonics whereas the basis consist of plane waves in IR region similar to PW-PP method with a cut off value of 50 Ry and charge density cut-off value of 800 Ry were used to expand the kinetic energy to describe the Kohn–Sham orbitals. Whereas, the energy convergence in the FP-LAPW method was achieved by expanding the plane wave functions in the IR with a cut off $R_{MT} \times K_{max} = 8$, where R_{MT} denotes the smallest muffin-tin sphere radius and K_{max} gives the maximum value of wave vector (K) in the plane wave expansion. The MT sphere radii (R_{MT}) used were 2.42, 2.30, 2.00, 2.22 and 2.50 (in a.u.) for Mn, Sc, Si, Ge and Sn, respectively. The potential inside the MT sphere and the non-spherical contributions to the charge density were expanded up to $l_{max} = 14$, whereas the potential and charge density were expanded as a Fourier series with the wave vectors up to $G_{max} = 14$. A uniform grid of $16 \times 16 \times 16$ automatically generated k-points following the convention of Monkhorst and Pack[71] centred at Γ-point for integration over the Brillouin zone was considered with energy convergence of 10^{-6} Ry. We have used the spin polarized Perdew–Burke–Ernzerhof scheme of generalized gradient approximation (PBE-GGA)[72] for the exchange correlation functional by treating onsite strong correlation of the 3d electrons by Coulomb repulsion U term (GGA+U).[73–76] The system dependent U term is calculated based on Hubbard Hamiltonian model (eqn (1)) for the onsite Coulomb repulsion.[55,67,68]

$$H_{Hub} = t \sum_{i,j>,\sigma} \left(c^{\dagger}_{i,\sigma} c_{j,\sigma}\right) + U \sum_{i} n_{i,\uparrow} n_{i,\downarrow} \quad (1)$$

where i,j denotes the nearest-neighbour atomic sites, $c^{\dagger}_{i,\sigma} c_{i,\sigma}$ are creation and annihilation operators, creating and annihilating an electron at atomic site i with spin $\sigma = \uparrow$ or $\downarrow$ and $n_{i,\sigma}$ is the number operator. In case of strongly localized electrons, the electrons hopes from one site to another with hoping amplitude t and is the single particle energy term of the total energy. U is the on-site Coulomb repulsion between electrons of the same atom which is proportional to the product of occupation numbers of atomic states on the same site. Gunnarsson scheme[77] was used to calculate the parameter U, in which the atoms are considered to be embedded in polarized surrounding with the onsite energies taken to be zero, then U will be the energy required to take the electron from one atom to other. If E_I and E_A are the ionization potential and electron affinity of the N electron system, then 'U' (eqn (2)) is given as[78]

$$U = E_I - E_A = (E^{N-1} - E^N) - (E^N - E^{N+1}) \quad (2)$$

where, $E^{N(\pm 1)}$ are the ground state energies. In our study, for calculation of U value, we have used a $2 \times 2 \times 2$ supercell and the d occupancies for 3d ions were fixed at integral values by removing the hoping whereas the hoping integral d shell of the central transition ion were set to zero. The calculated values of U in present system of study was found to be $U_{Mn} = 1.973$ eV and $U_{Sc} = 0.435$ eV for Mn and Sc respectively.

3. Results and discussion

3.1 Structural optimization and elastic properties

Full Heusler alloys X_2YZ where X and Y are transition elements and Z is an sp element crystallizes in a cubic fcc structure with four atomic basis at $4a$ (0, 0, 0), $4b$ $\left(\frac{1}{2}, \frac{1}{2}, \frac{1}{2}\right)$, $4c$ $\left(\frac{1}{4}, \frac{1}{4}, \frac{1}{4}\right)$ and $4d$ $\left(\frac{3}{4}, \frac{3}{4}, \frac{3}{4}\right)$. Depending on the number of valence electrons of X atom being greater than or less than that of Y atom, the alloy can crystallize in either Cu_2MnAl type structure (space group $Fm\bar{3}m$) with X in $4a$ and $4b$ positions, Y in $4c$ and Z in $4d$ position or in Hg_2CuTi type structure (space group $F\bar{4}3m$) with X occupying $4a$ and $4c$ positions, Y in $4b$ and Z in 4d positions respectively. The Cu_2MnAl structure is also known as $L2_1$ structure or regular Heusler alloys whereas the Hg_2CuTi structure is known as XA structure or inverse Heusler alloys.

The type of structure depending on the valence electron count rule as described above is generally true for almost all the Heusler alloys however, Galehgirian *et al.* found Ti_2VZ(Z = Al, Ga and In) to be stable in Hg_2CuTi type structure,[79] against the above rule. Similarly Luo *et al.*[80] studied a series of X_2CuAl (X = Sc, Ti, V, Cr, Mn, Fe, Co, Ni) and found that although all should crystallize in XA structure according to above rule, some of the alloys crystallizes in Cu_2MnAl type and the others in Hg_2CuTi type structure. In this context, an interesting result was reported by Bensiad *et al.* in series of Mn_2RhZ (Z = Si, Ge and Sn), where Mn_2RhSi and Mn_2RhGe were found to crystallize in Cu_2MnAl type structure whereas the Mn_2RhSn crystallizes in Hg_2CuTi type structure.[81] Hence, following the above discrepancies, the sample alloys were optimized for both the structure in magnetic (M) and non magnetic phases in both Cu_2MnAl and Hg_2CuTi type structure to understand equilibrium structure. The variation of total energy as a function of lattice constant fitted into empirical Murnaghan's equation of state is presented in Fig. 1a. Due to similar nature of the curves, we have presented the curve only for Mn_2ScSi (Fig. 1b) and the energy difference $\Delta E = E_{Fm\bar{3}m} - E_{F\bar{4}3m}$ between the Cu_2MnAl and Hg_2CuTi type structure are summarized in Table 1 which depicts, that the magnetic phase of Cu_2MnAl type structure are energetically stable and has been used to further explore their physical properties at optimized lattice constant (Table 1). The addition of bigger size atom (Si to Sn) expand the overall size of the crystal in consistent to analogous Fe_2MnZ (Z = Si, Ge and Sn)[82] and by Mn_2RhZ (Z = Si, Ge and Sn).[81]

The hypothetical compounds Mn_2ScZ (Z = Si, Ge and Sn) are thermodynamically stable and their experimental synthesis is also possible as predicted from formation energy (E_{form}) (Table 1) obtained from relation[83]

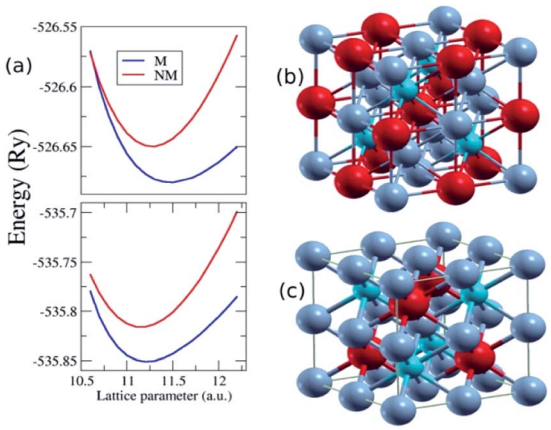

Fig. 1 (a) Volume optimization curve in the magnetic (M) and non-magnetic (NM) phase for Hg_2CuTi type (upper panel) and Cu_2MnAl type structure (lower panel), (b) Hg_2CuTi type and (c) Cu_2MnAl type crystal structure (colour scheme, Mn = grey, Sc = red and Z = blue).

Table 1 Optimized lattice constant (a), total energy (E_o), difference in ground state energy (ΔE) between Cu_2MnAl and Hg_2CuTi type structure in magnetic phases and formation energy (E_{form}) of Mn_2ScZ (Z = Si, Ge and Sn)

Z	a (Å)	ΔE (Ry)	E_o (Ry)	E_{form} (eV)
Si	5.949	−9.133	−535.851	−3.209
Ge	6.036	−5.372	−701.9321	−5.105
Sn	6.396	−2.028	−688.582	−3.188

$$E_{form} = \frac{1}{4}\{E_o - (2E_{Mn} + E_{Sc} + E_Z)\} \quad (3)$$

where, E_o is the ground state energy of Mn_2ScZ (Z = Si, Ge and Sn) and $E_{Mn} = -2317.0374$ Ry, $E_{Sc} = -1528.139$ Ry, and E_Z (Si = −579.734 Ry, Ge = −4192.046 Ry and Sn = −12358.061 Ry) are the equilibrium energy of Mn, Sc, and Z (Si, Ge and Sn) respectively in their solid state.

Elastic constants can be used to furnish the critical informations regarding the mechanical stability of a solid structure against the arbitrary deformation and moreover, the physical properties such as propagation of elastic waves in normal mode, specific heat, chemical bonds, hardness and Debye temperature are also related to them. The strain was used to determine the independent elastic constants (C_{ij}) in such a way that the total volume of the system remains constant. The details about the type of strains applied are given in ref. 84. The symmetry of the cubic crystal reduces the total number of independent elastic constants into 3 *i.e.* C_{11}, C_{12} and C_{44} and they are the elements of elastic stiffness matrix of order 6×6, with 6 eigen values. However there are only 3 different eigen values; $C_{11} + 2C_{12}$ (non-degenerate), $C_{11} - C_{12}$ (two fold degenerate) and C_{44} (threefold degenerate), which corresponds to bulk, the tetragonal shear and the shear moduli of the crystal and the cubic crystals becomes unstable if these values become negative. The listed elastic constants in Table 2 are found to satisfy the above stability criteria as mentioned by Born and Huang.[85]

The bulk modulus (B) and the isotropic shear modulus (G) has been calculated using the Voigt–Reuss and Hill[86] approximation as[84]

$$B = \frac{1}{6}(C_{11} + 2C_{12}) \quad (4)$$

$$G = \frac{1}{2}(G_V + G_R) \quad (5)$$

where,

$$G_V = \frac{1}{5}(C_{11} - C_{12} + 3C_{44}) \quad (6)$$

$$G_R = 5\frac{(C_{11} - C_{12})C_{44}}{3(C_{11} - C_{12}) + 4C_{44}} \quad (7)$$

B defines the hardness of the material and characterizes the resistance of the material to fracture whereas G gives the resistant to plastic deformations. One can find from the table that $B > G$, indicating the prominence of shear modulus in the stability of the sample materials. Also the computed values of B and G are comparable with of Mn_2ZrSi ($B = 187.015$ GPa, $G = 80.249$ GPa), Mn_2ZrGe ($B = 175.478$ GPa, $G = 71.088$ GPa)[87] and Fe_2MnSi ($B = 228$ GPa, $G = 73$ GPa).[82]

Using the above B and G, one can find the Young's modulus (E) and Poisson's ratio (ν) as[84]

$$E = \frac{9GB}{3B + G} \quad (8)$$

$$\nu = \frac{1}{2}\left(\frac{3B - 2G}{3B + G}\right) \quad (9)$$

E is the ratio of tensile stress to tensile strain that measures the stiffness of the material and here Mn_2ScSn is the stiffest.

Table 2 Calculated independent elastic constants (C_{ij}), bulk modulus (B), shear modulus (G), Young modulus (E), elastic anisotropy (A), Poisson's ratio (ν), Cauchy's pressure (C^P), Pugh's ratio (B/G) longitudinal velocity (υ_l), transverse velocity (υ_t), average sound velocity (υ_m) and Debye temperature (Θ_D)

Parameters	Mn_2ScSi	Mn_2ScGe	Mn_2ScSn
C_{11}	220.449	222.949	227.029
C_{12}	129.05	138.855	145.449
C_{44}	79.128	94.923	103.608
$C_{11} - C_{12}$	91.399	84.094	81.58
$C_{11} + 2C_{12}$	478.549	500.659	517.927
B (GPa)	159.517	166.886	172.642
G (GPa)	63.487	68.464	71.297
E (GPa)	168.152	180.683	188.010
A	1.731	2.258	2.540
ν	0.324	0.320	0.318
C^P	49.922	43.932	41.841
(B/G)	2.5126	2.43758	2.42145
υ_l (m s^{-1})	13012.672	12238.046	11753.483
υ_t (m s^{-1})	3335.374	6302.145	6065.602
υ_m (m s^{-1})	7434.818	7057.058	6791.246
Θ_D (K)	937.491	878.227	826.381

The ν determines the nature of atomic bonding present in the material and its critical value is 0.26 (ref. 88) separating the covalent and ionic nature. The Pugh's ratio (B/G) with a critical value of 1.75 (ref. 84) predicts their ductile with ionic type of bonding. One can also determine the type of atomic bonding by calculating C^P with large negative value for directional covalent bonding whereas a positive value for non-directional metallic bonding and all the materials are found to show non-directional metallic bonding in the present study.

$$C^P = C_{12} - C_{44} \quad (10)$$

$$A = \frac{2C_{44}}{C_{11} - C_{12}} \quad (11)$$

The anisotropy factor A, which is the measure of the degree of anisotropy of the material and the deviation from unity indicates the probability of development of cracks during the crystal growth process. Although it deviates from unity in present case, it is quite less when compared to Fe_2MnSi (7.21), Fe_2MnGe (8.30) and Fe_2MnSn (25.88).[82]

The Debye temperature (Θ_D) is an important elastic parameter which is related to many thermodynamic properties and its estimation from elastic constants is expected to reflect the true value at low temperatures because in such conditions the crystal vibration is of acoustic type. It can be calculated from the average mean velocity (υ_m) as:[84]

$$\Theta_D = \frac{h}{k_B}\left(\frac{3n}{4\pi V_a}\right)^{\frac{-1}{3}}\upsilon_m \quad (12)$$

where h, k_B, n and V_a are Planck's constant, Boltzmann's constant, number of atoms per formula unit and atomic volume of the alloy respectively. One can find that the Θ_D decreases with the increase in atomic size of Z (Si to Sn) atom in Mn_2ScZ (Z = Si, Ge and Sn) as expected because on addition of heavier mass Z atom, the υ_m will decrease as observed in analogous Fe_2MnZ (Z = Si, Ge and Sn).[82]

3.2 Electronic structure and magnetic properties

Study of electronic structure in context of half-metallicity have been performed earlier in analogous system like Fe_2MnZ, Mn_2RhZ, Mn_2TiZ, Mn_2ZrZ and Co_2MnZ (Z= Si, Ge and Sn)[81,82,87,89,90] where the decrease in HM gap or even lost of half-metallicity with increase in size of Z atom has been reported. To check similar feature in the sample materials and understand their effect we have calculated spin-polarized electronic band structure along the high-symmetric direction of the Brillouin zone (BZ) (Fig. 2) and corresponding density of states (DOS) (Fig. 3) in the equilibrium configuration. In present study, the total number of valence electron is 21, thus according to Slater Pauling rule (SP) of 24 we have spin down electron as the majority spin and spin up electron as minority spin.[91] From the figures one can find both Mn_2ScSi and Mn_2ScGe shows half metallic structure with continuous bands and DOS crossing the E_F for majority spin whereas a gap occurs at E_F for minority spin. For Mn_2ScSn, the band crosses E_F for both the spin

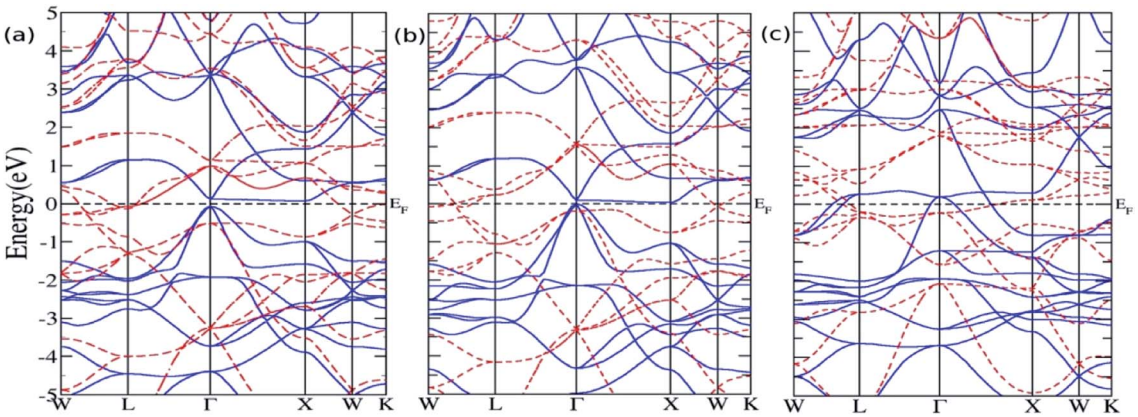

Fig. 2 Energy band structure of (a) Mn_2ScSi, (b) Mn_2ScGe and (c) Mn_2ScSn (colour scheme, solid blue lines = minority spin and dash red lines = majority spin).

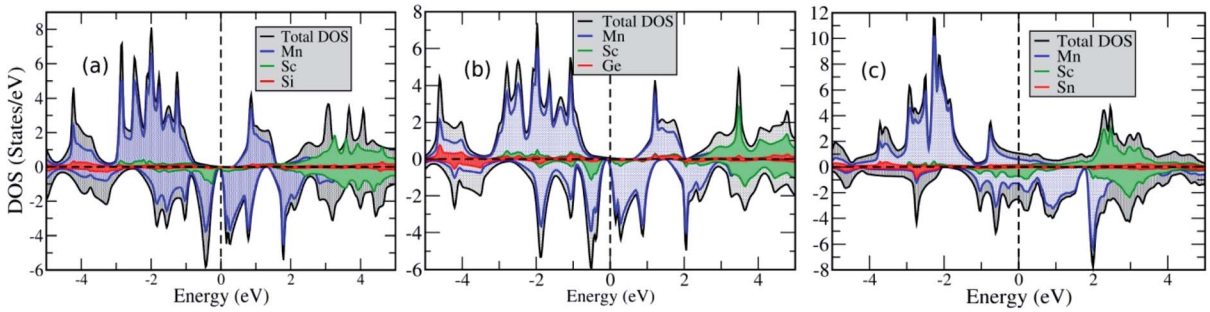

Fig. 3 Total density of states of (a) Mn_2ScSi (b) Mn_2ScGe and (c) Mn_2ScSn.

channels, showing a metallic nature. Moreover the profile of the DOSs and bands are similar for two HMs whereas, completely different for metallic Mn_2ScSn. There are many peaks in the minority DOS around -2 eV below E_F for Mn_2ScSi and Mn_2ScGe which is visible as flat regions in their corresponding bands. These peaks merge to form a more prominent one in magnitude in case of Mn_2ScSn as seen from a broader flat band at Γ point. Moreover the minority DOS peaks above E_F around 1 eV for Mn_2ScSi and Mn_2ScGe moves below E_F at around -0.8 eV in case of Mn_2ScSn, thus destroying the half-metallicity. This feature is again visible as flat regions between 0–1 eV for Mn_2ScSi and Mn_2ScGe at Γ and L point which are pushed below E_F for Mn_2ScSn. Moreover the bands between -4 eV to -3 eV in both the spins for Mn_2ScSi and Mn_2ScGe at Γ are pushed towards the E_F in case of Mn_2ScSn as seen in their respective DOSs. The DOS also reveals the prominent role of Mn around the E_F in comparison to Sc and Z (Si, Ge and Sn) atoms in all the three sample materials. Moreover the asymmetry in the bands and DOS between majority and minority spin of these alloys is mainly due to Mn atoms. For the HMs, the band gaps are indirect with the maximum of valence band and the minimum of conduction bands occurring at Γ and X points of the BZ respectively. The band gaps are very narrow, 0.151 eV and 0.051 eV for Mn_2ScSi and Mn_2ScGe respectively. And as the size of the Z atom increases from Si to Ge, the band gap decreases and eventually disappears for Sn in consistent analogous Fe_2MnZ (Z = Si, Ge and Sn),[82] Mn_2TiZ (Z = Si, Ge and Sn)[89] and Co_2MnZ (Z = Ge and Sn).[90] This indicate the prominence of size of Z atoms in Mn_2YZ compounds for controlling the size of the lattice (Table 1) and eventually determining the strength of interaction between the transition elements and overlap of d orbitals resulting in half-metallicity.[40] So, with the addition of bigger atomic radius Z, the lattice constant increases and the overlap of d orbitals reduces and ultimately results in loss of HM in Mn_2ScSn.

Further analysis of electronic structure is done by studying their partial density of states (PDOS) as presented in Fig. 4, which gives us insight into the hybridization between atomic orbitals and formation of energy gap in minority spin resulting in HM as explained by Galanakis *et al.*[92] in full Heusler alloys with $L2_1$ structure. The sp Z atom forms one s and three p bands fully occupied by electrons. The s state forms band in the core region (not shown in the PDOS) well below from the E_F and are well separated from the d bands, whereas on the other hand, the p electrons contribute at around -4 eV and are not completely separated from the d bands. The PDOS clearly shows that around E_F, it is the d electrons which play the predominant role and as suggested by Galanakis,[92] we shall consider formation of band gap in two steps. The whole crystal has tetrahedral symmetry (T_d) but the Mn atoms at 4a and 4b positions obey octahedral symmetry (O_h) with respect to each other and d orbitals splits into doubly degenerate e_g and triply

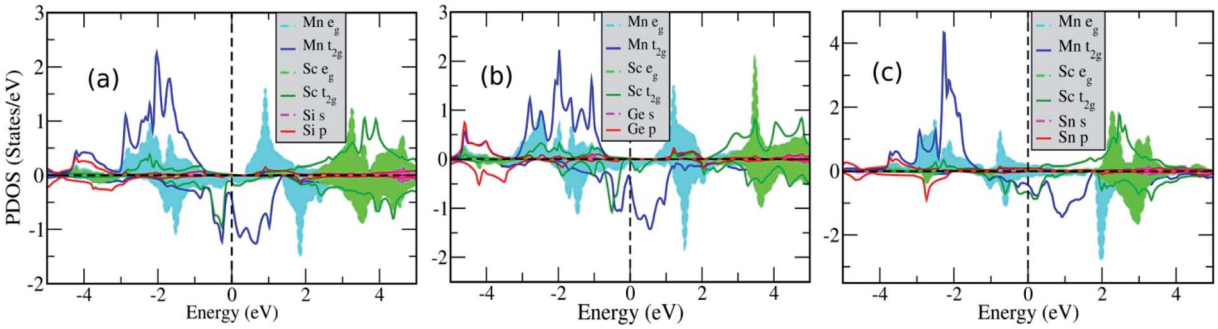

Fig. 4 Partial density of states (a) Mn_2ScSi (b) Mn_2ScGe and (c) Mn_2ScSn (dashed lines are filled with same colour).

degenerate t_{2g}. Therefore, in first step we should consider the interaction of Mn atoms which is schematically shown in Fig. 5. Due to symmetry, e_g of Mn at 4*a* can hybridize only with e_g of Mn at 4*b* and t_{2g} orbitals follow the same trend giving 2 e_g and 3 t_{2g} bonding and 2 e_u and 3 t_{1u} anti-bonding orbitals (Fig. 5a). The numeral figures before the states give the degeneracy of the orbitals. Now in the second step, these Mn–Mn orbitals again combine with e_g and t_{2g} orbitals of Sc atom (O_h) at 4*c* to give 2 e_g and 3 t_{2g} bonding below and 2 e_g and 3 t_{2g} anti-bonding orbitals above E_F respectively. These anti-bonding e_g and t_{2g} orbitals can be seen as peaks in the minority spin PDOS between 3 to 4 eV and the degeneracy of orbitals can be verified by counting the number of bands in the same energy range at Γ point in the bands. The bonding t_{2g} orbitals peaks just below −2 eV in the minority PDOS and which can be seen at Γ point in the bands whereas the e_g bonding orbitals peak around −4 eV and is correspondingly appears as doubly degenerate band at Γ point in the band. The 2 e_u and 3 t_{1u} orbitals of Mn–Mn hybridization cannot couple with the d orbitals of Sc atom due to their different symmetry and the gap is formed between these non-bonding orbitals as seen from the peaks in the valence band edge and conduction band edge in the PDOS. In the PDOS the representation of e_u and t_{1u} remains as e_g and t_{2g} respectively and can be seen as doubly degenerate and triply degenerate bands just above and below E_F minority spin bands.

For regular Heusler alloy with $L2_1$ structure, the SP rule for total magnetic moment (M_T) per formula unit for HMs is $M_T = (N_T - 24)\ \mu_B$, where N_T is the total number of valence electron. Thus in the present study with $N_T = 21$, we expect a M_T of $-3\ \mu_B$ as presented in Table 3. The negative moment comes from the fact that gap occurs in the minority spin states and DOS at E_F of majority spin states. The total magnetic moment (M_T) per formula unit for Mn_2ScSi and Mn_2ScGe is almost an integral value of $-3.0\ \mu_B$ which also confirms the half-metallic nature in these two compounds. Also, the M_T for Mn_2ScSn decreases to $-5.93\ \mu_B$ deviating from SP rule and clearly indicating the loss of HM and such similar behaviour in magnetic moment was reported by Jain *et al.*[82] in 27 valence electrons system Fe_2MnZ (Z = Si, Ge and Sn) with 5.73 μ_B for Fe_2MnSn and 3.0 μ_B for the rest. Again, Mn predominantly contributes to the M_T and determines the magnetic properties of these alloys whereas the contribution from Sc and Z atom to M_T is comparatively less as presented by partial magnetic moments in Table 3. Moreover, the magnetic moments of Mn and Sc are aligned in opposite direction with different strength showing the ferrimagnetic ordering of moments. These magnetic behaviours can be understood by examining the DOS (Fig. 3) and PDOS (Fig. 4) of these compounds and this asymmetry in the DOS between majority and minority spins reflects the origin of magnetism. The PDOS explains the opposite alignment of magnetic moment of Mn and Sc atoms in these compounds. The d states of Mn emerge in −2.0 eV below E_F in minority spin, whereas around 0.8 eV above E_F in majority spin. However, in case of Sc, the d states emerges slightly more in majority spin than in minority spin around −2.0 eV below E_F. As a consequence, it is the majority spin of Mn atoms which is predominantly unoccupied giving a large and opposite magnetic moment to Mn in comparison to that of Sc for HMs. This situation is magnified in case of metallic Mn_2ScSn, where the asymmetry and occupancy of d states of Mn and Sc in majority and minority states is distinctly visible and results in large magnetic moment of Mn. Here, Table 3 also shows that with increase in the lattice

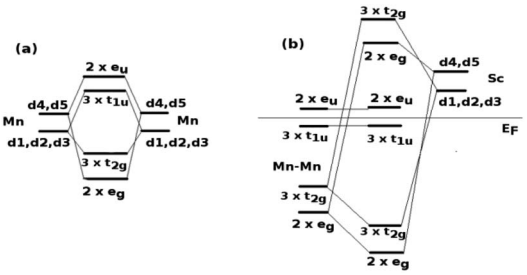

Fig. 5 Scheme of d orbitals of Mn_2ScZ (Z = Si, Ge and Sn) in Cu_2MnAl configuration: (a) Mn–Mn and (b) Mn–Mn–Sc hybridization.

Table 3 Partial and total magnetic moment (M_T) per formula unit of Mn_2ScZ (Z = Si, Ge and Sn)

Magnetic moment (in μ_B)	Mn	Sc	Z	Total (M_T)
Mn_2ScSi	−1.606	0.159	0.084	−2.99
Mn_2ScGe	−1.646	0.213	0.073	−2.98
Mn_2ScSn	−3.169	0.298	0.065	−5.93

parameter *a* which increases with the atomic radius of Z atom *i.e.* on going from Mn_2ScSi to Mn_2ScSn, the magnetic moment of Mn keeps on decreasing whereas that of Sc increases. This clearly indicates the role of size of Z atom on determining the size of crystal structure and thereby affecting the strength of coupling interaction of moments in these alloys.

4. Conclusions

The ground state electronic and magnetic properties of new Heusler alloys Mn_2ScZ (Z = Si, Ge and Sn) have been investigated using density functional theory with the implementation of Hubbard correction term of Coulomb repulsion *U* to the generalized gradient approximation for exchange correlation functional. All these sample materials were found to crystallize in Cu_2MnAl type structure and the stability as well as the possibility of experimental synthesis was determined by calculating the formation energy and from independent elastic constants. The analysis of electronic structure predicted half-metallic character for Mn_2ScSi and Mn_2ScGe whereas metallic character for Mn_2ScSn. The lost of HM in Mn_2ScSn is due to the increase in size of crystal which comes from the size of Z atom resulting in lesser overlap of d orbitals consistent to previous reports of analogous alloys. The HM and metallic nature was also confirmed from the study of magnetic properties which showed anti-parallel alignment of magnetic moments of Mn with Sc resulting in ferrimagnetic ordering in these alloys. Moreover, the total magnetic moments per formula unit for half-metals were found to be 3.00 μ_B which comes from Slating–Pauling rule of 24 and for metal was found to be far more than predicted by above rule, thereby confirming HM in Mn_2ScSi and Mn_2ScGe whereas metallic nature for Mn_2ScSn. Analysis of both electronic and magnetic properties reveals the prominence of size of sp element in these alloys.

Conflicts of interest

There are no conflicts to declare.

Notes and references

1 I. Žutić, J. Fabian and S. D. Sarma, Spintronics: Fundamentals and applications, *Rev. Mod. Phys.*, 2004, **76**(2), 323.
2 S. A. Wolf, D. D. Awschalom, R. A. Buhrman, J. M. Daughton, S. Von Molnar, M. L. Roukes and D. M. Treger, Spintronics: a spin-based electronics vision for the future, *science*, 2001, **294**(5546), 1488–1495.
3 K. L. Wang, J. G. Alzate and P. K. Amiri, Low-power non-volatile spintronic memory: STT-RAM and beyond, *J. Phys. D: Appl. Phys.*, 2013, **46**(7), 074003.
4 H. Lee, F. Ebrahimi, P. K. Amiri and K. L. Wang, Low-power, high-density spintronic programmable logic with voltage-gated spin Hall effect in magnetic tunnel junctions, *IEEE Magn. Lett.*, 2016, **7**, 1–5.
5 W. Zhao, E. Belhaire, C. Chappert and P. Mazoyer, Spintronic device based non-volatile low standby power SRAM, in *2008 IEEE Computer Society Annual Symposium on VLSI*, IEEE, 2008, pp. 40–45.
6 K. Nikolaev, P. Kolbo, T. Pokhil, X. Peng, Y. Chen, T. Ambrose and O. Mryasov, "All-Heusler alloy" current-perpendicular-to-plane giant magnetoresistance, *Appl. Phys. Lett.*, 2009, **94**(22), 222501.
7 Y. Sakuraba, A. M. Hattori, M. Oogane, Y. Ando, H. Kato, A. Sakuma and H. Kubota, Giant tunneling magnetoresistance in $Co_2MnSi/AlO/Co_2MnSi$ magnetic tunnel junctions, *Appl. Phys. Lett.*, 2006, **88**(19), 192508.
8 S. Tsunegi, Y. Sakuraba, M. Oogane, K. Takanashi and Y. Ando, Large tunnel magnetoresistance in magnetic tunnel junctions using a Co_2MnSi Heusler alloy electrode and a MgO barrier, *Appl. Phys. Lett.*, 2008, **93**(11), 112506.
9 T. Ishikawa, T. Marukame, H. Kijima, K. I. Matsuda, T. Uemura, M. Arita and M. Yamamoto, Spin-dependent tunneling characteristics of fully epitaxial magnetic tunneling junctions with a full-Heusler alloy Co_2MnSi thin film and a MgO tunnel barrier, *Appl. Phys. Lett.*, 2006, **89**(19), 192505.
10 Y. Wang, J. Zheng, Z. Ni, R. Fei, Q. Liu, R. Quhe and J. Lu, Half-metallic silicene and germanene nanoribbons: towards high-performance spintronics device, *Nano*, 2012, **7**(05), 1250037.
11 H. X. Liu, Y. Honda, T. Taira, K. I. Matsuda, M. Arita, T. Uemura and M. Yamamoto, Giant tunneling magnetoresistance in epitaxial $Co_2MnSi/MgO/Co_2MnSi$ magnetic tunnel junctions by half-metallicity of Co_2MnSi and coherent tunneling, *Appl. Phys. Lett.*, 2012, **101**(13), 132418.
12 J. Y. T. Wei, N. C. Yeh, R. P. Vasquez and A. Gupta, Tunneling evidence of half-metallicity in epitaxial films of ferromagnetic perovskite manganites and ferrimagnetic magnetite, *J. Appl. Phys.*, 1998, **83**(11), 7366–7368.
13 K. Ramesha, R. Seshadri, C. Ederer, T. He and M. A. Subramanian, Experimental and computational investigation of structure and magnetism in pyrite $Co_{1-x}Fe_xS_2$: chemical bonding and half-metallicity, *Phys. Rev. B: Condens. Matter Mater. Phys.*, 2004, **70**(21), 214409.
14 J. H. Park, S. K. Kwon and B. I. Min, Half-metallic antiferromagnetic double perovskites: $LaAVRuO_6$ (A= Ca, Sr, and Ba), *Phys. Rev. B: Condens. Matter Mater. Phys.*, 2002, **65**(17), 174401.
15 I. Galanakis and E. Şaşıoğlu, High T_C half-metallic fully-compensated ferrimagnetic Heusler compounds, *Appl. Phys. Lett.*, 2011, **99**(5), 052509.
16 S. Wurmehl, G. H. Fecher, H. C. Kandpal, V. Ksenofontov, C. Felser and H. J. Lin, Investigation of Co_2FeSi: The Heusler compound with highest Curie temperature and magnetic moment, *Appl. Phys. Lett.*, 2006, **88**(3), 032503.
17 I. Galanakis, P. Mavropoulos and P. H. Dederichs, Electronic structure and Slater–Pauling behaviour in half-metallic Heusler alloys calculated from first principles, *J. Phys. D: Appl. Phys.*, 2006, **39**(5), 765.
18 K. Özdoğan, E. Şaşıoğlu and I. Galanakis, Slater-Pauling behavior in LiMgPdSn-type multifunctional quaternary Heusler materials: half-metallicity, spin-gapless and

magnetic semiconductors, *J. Appl. Phys.*, 2013, **113**(19), 193903.

19 S. Chadov, X. Qi, J. Kübler, G. H. Fecher, C. Felser and S. C. Zhang, Tunable multifunctional topological insulators in ternary Heusler compounds, *Nat. Mater.*, 2010, **9**(7), 541.

20 T. Graf, S. S. Parkin and C. Felser, Heusler compounds: a material class with exceptional properties, *IEEE Trans. Magn.*, 2011, **47**(2), 367–373.

21 A. K. Nayak, M. Nicklas, S. Chadov, P. Khuntia, C. Shekhar, A. Kalache and U. Zeitler, Design of compensated ferrimagnetic Heusler alloys for giant tunable exchange bias, *Nat. Mater.*, 2015, **14**(7), 679.

22 S. Fujii, S. Ishida and S. Asano, A half-metallic band structure and Fe_2MnZ (Z= Al, Si, P), *J. Phys. Soc. Jpn.*, 1995, **64**(1), 185–191.

23 S. Ishida, S. Mizutani, S. Fujii and S. Asano, Theoretical prediction of materials to preserve high spin polarization against chemical disorder, *Mater. Trans.*, 2006, **47**(1), 31–37.

24 L. Hongzhi, Z. Zhiyong, M. Li, X. Shifeng, L. Heyan, Q. Jingping and W. Guangheng, Electronic structure and magnetic properties of Fe_2YSi (Y = Cr, Mn, Fe, Co, Ni) Heusler alloys: a theoretical and experimental study, *J. Phys. D: Appl. Phys.*, 2007, **40**(22), 7121.

25 X. J. Zhang, Z. H. Liu, Y. J. Zhang, H. Y. Liu, G. D. Liu, Y. T. Cui and X. Q. Ma, Theoretical and experimental study of the phase formation for Ti_2YAl and $Ti_2Y'Ga$ (Y = Co, Fe; Y′= Cr, Fe), *Intermetallics*, 2016, **73**, 26–30.

26 W. H. Wang, M. Przybylski, W. Kuch, L. I. Chelaru, J. Wang, Y. F. Lu and J. Kirschner, Magnetic properties and spin polarization of Co_2MnSi Heusler alloy thin films epitaxially grown on GaAs (001), *Phys. Rev. B: Condens. Matter Mater. Phys.*, 2005, **71**(14), 144416.

27 S. Mizukami, D. Watanabe, M. Oogane, Y. Ando, Y. Miura, M. Shirai and T. Miyazaki, Low damping constant for Co_2FeAl Heusler alloy films and its correlation with density of states, *J. Appl. Phys.*, 2009, **105**(7), 07D306.

28 V. Asvini, G. Saravanan, R. K. Kalaiezhily, M. M. Raja and K. Ravichandran, Effect of film thickness on soft magnetic behaviour of Fe_2CoSi Heusler alloy for spin transfer torque device applications, in *AIP Conference Proceedings*, AIP Publishing, 2018, p. 130051, Vol. 1942, No. 1.

29 M. P. Geisler, M. Meinert, J. Schmalhorst, G. Reiss and E. Arenholz, Multiple phases in sputtered Cr_2CoGa films, *J. Alloys Compd.*, 2014, **598**, 213–216.

30 R. Knut, P. Svedlindh, O. Mrvasov, K. Gunnarsson, P. Warnicke, D. A. Arena, M. Bjorck, A. J. Dennison, A. Sahoo, S. Mukherjee and D. D. Sarma, Interface characterization of Co_2MnGe/Rh_2CuSn Heusler multilayers, *Phys. Rev. B: Condens. Matter Mater. Phys.*, 2013, **88**(13), 134407.

31 H. G. Zhang, C. Z. Zhang, W. Zhu, E. K. Liu, W. H. Wang, H. W. Zhang, J. L. Cheng, H. Z. Luo and G. H. Wu, Significant disorder-induced enhancement of the magnetization of Fe_2CrGa by ball mining, *J. Appl. Phys.*, 2013, **114**(1), 013903.

32 J. Winterlik, S. Chadov, A. Gupta, V. Alijani, T. Gasi, K. Filsinger and J. Kübler, Design Scheme of New Tetragonal Heusler Compounds for Spin-Transfer Torque Applications and its Experimental Realization, *Adv. Mater.*, 2012, **24**(47), 6283–6287.

33 C. Felser, V. Alijani, J. Winterlik, S. Chadov and A. K. Nayak, Tetragonal Heusler compounds for spintronics, *IEEE Trans. Magn.*, 2013, **49**(2), 682–685.

34 A. K. Nayak, C. Shekhar, J. Winterlik, A. Gupta and C. Felser, Mn_2PtIn: A tetragonal Heusler compound with exchange bias behavior, *Appl. Phys. Lett.*, 2012, **100**(15), 152404.

35 A. K. Nayak, M. Nicklas, S. Chadov, C. Shekhar, Y. Skourski, J. Winterlik and C. Felser, Large zero-field cooled exchange-bias in bulk Mn_2PtGa, *Phys. Rev. Lett.*, 2013, **110**(12), 127204.

36 C. Felser, L. Wollmann, S. Chadov, G. H. Fecher and S. S. Parkin, Basics and prospective of magnetic Heusler compounds, *APL Mater.*, 2015, **3**(4), 041518.

37 G. D. Liu, X. F. Dai, H. Y. Liu, J. L. Chen, Y. X. Li, G. Xiao and G. H. Wu, Mn_2CoZ (Z = Al, Ga, In, Si, Ge, Sn, Sb) compounds: Structural, electronic, and magnetic properties, *Phys. Rev. B: Condens. Matter Mater. Phys.*, 2008, **77**(1), 014424.

38 P. Entel, M. Siewert, M. E. Gruner, H. C. Herper, D. Comtesse, R. Arróyave and F. Albertini, Complex magnetic ordering as a driving mechanism of multifunctional properties of Heusler alloys from first principles, *Eur. Phys. J. B*, 2013, **86**(2), 65.

39 M. Meinert, J. M. Schmalhorst and G. Reiss, Ab initio prediction of ferrimagnetism, exchange interactions and Curie temperatures in Mn_2TiZ Heusler compounds, *J. Phys.: Condens. Matter*, 2010, **23**(3), 036001.

40 M. Meinert, J. M. Schmalhorst and G. Reiss, Exchange interactions and Curie temperatures of Mn_2CoZ compounds, *J. Phys.: Condens. Matter*, 2011, **23**(11), 116005.

41 T. Gasi, A. K. Nayak, J. Winterlik, V. Ksenofontov, P. Adler, M. Nicklas and C. Felser, Exchange-spring like magnetic behavior of the tetragonal Heusler compound Mn_2FeGa as a candidate for spin-transfer torque, *Appl. Phys. Lett.*, 2013, **102**(20), 202402.

42 R. Weht and W. E. Pickett, Half-metallic ferrimagnetism in Mn_2VAl, *Phys. Rev. B: Condens. Matter Mater. Phys.*, 1999, **60**(18), 13006.

43 T. Kubota, K. Kodama, T. Nakamura, Y. Sakuraba, M. Oogane, K. Takanashi and Y. Ando, Ferrimagnetism in epitaxially grown Mn_2VAl Heusler alloy investigated by means of soft x-ray magnetic circular dichroism, *Appl. Phys. Lett.*, 2009, **95**(22), 222503.

44 H. Luo, Z. Zhu, G. Liu, S. Xu, G. Wu, H. Liu and Y. Li, Prediction of half-metallic properties for the Heusler alloys Mn_2CrZ (Z = Al, Ga, Si, Ge, Sb): A first-principles study, *J. Magn. Magn. Mater.*, 2008, **320**(3–4), 421–428.

45 H. Zenasni, H. I. Faraoun and C. Esling, First-principle prediction of half-metallic ferrimagnetism in Mn-based full-Heusler alloys with highly ordered structure, *J. Magn. Magn. Mater.*, 2013, **333**, 162–168.

46 H. Z. Luo, H. W. Zhang, Z. Y. Zhu, L. Ma, S. F. Xu, G. H. Wu and H. B. Xu, Half-metallic properties for the Mn_2FeZ (Z =

Al, Ga, Si, Ge, Sb) Heusler alloys: A first-principles study, *J. Appl. Phys.*, 2008, **103**(8), 083908.

47 V. V. Sokolovskiy, M. A. Zagrebin, Y. A. Sokolovskaya and V. D. Buchelnikov, Structural and Magnetic Properties of Mn_2NiZ (Z= Ga, In, Sn, Sb) Heusler Alloys from Ab initio Calculations, in *Solid State Phenomena*, Trans Tech Publications, 2015, Vol. 233, pp. 229–232.

48 L. Wollmann, S. Chadov, J. Kübler and C. Felser, Magnetism in cubic manganese-rich Heusler compounds, *Phys. Rev. B: Condens. Matter Mater. Phys.*, 2014, **90**(1), 214420.

49 L. Wollmann, S. Chadov, J. Kübler and C. Felser, Magnetism in tetragonal manganese-rich Heusler compounds, *Phys. Rev. B: Condens. Matter Mater. Phys.*, 2015, **92**(6), 064417.

50 M. Tas, E. Şaşıoğlu, C. Friedrich, S. Blügel and I. Galanakis, Design of $L2_1$-type antiferromagnetic semiconducting full-Heusler compounds: A first principles DFT+GW study, *J. Appl. Phys.*, 2017, **121**(5), 053903.

51 S. S. Shastri and S. K. Pandey, Two functionals approach in DFT for the prediction of thermoelectric properties of Fe_2ScX (X= P, As, Sb) full Heusler compounds, arXiv preprint arXiv:1904.04322, 2019.

52 J. L. Da Silva, M. V. Ganduglia-Pirovano and J. Sauer, Formation of the cerium orthovanadate $CeVO_4$: DFT+*U* study, *Phys. Rev. B: Condens. Matter Mater. Phys.*, 2007, **76**(12), 125117.

53 M. Derzsi, P. Piekarz, P. T. Jochym, J. Łażewski, M. Sternik, A. M. Oleś and K. Parlinski, Effects of Coulomb interaction on the electronic structure and lattice dynamics of the Mott insulator Fe_2SiO_4 spinel, *Phys. Rev. B: Condens. Matter Mater. Phys.*, 2009, **79**(20), 205105.

54 A. I. Liechtenstein, V. I. Anisimov and J. Zaanen, Density-functional theory and strong interactions: Orbital ordering in Mott-Hubbard insulators, *Phys. Rev. B: Condens. Matter Mater. Phys.*, 1995, **52**(8), R5467.

55 V. I. Anisimov, J. Zaanen and O. K. Andersen, Band theory and Mott insulators: Hubbard *U* instead of Stoner I, *Phys. Rev. B: Condens. Matter Mater. Phys.*, 1991, **44**(3), 943.

56 I. de PR Moreira, F. Illas and R. L. Martin, Effect of Fock exchange on the electronic structure and magnetic coupling in NiO, *Phys. Rev. B: Condens. Matter Mater. Phys.*, 2002, **65**(15), 155102.

57 H. Tang, F. Levy, H. Berger and P. E. Schmid, Urbach tail of anatase TiO_2, *Phys. Rev. B: Condens. Matter Mater. Phys.*, 1995, **52**(11), 7771.

58 M. Sodupe, J. Bertran, L. Rodríguez-Santiago and E. J. Baerends, Ground State of the $(H_2O)^{2+}$ Radical Cation: DFT versus Post–Hartree−Fock Methods, *J. Phys. Chem. A*, 1999, **103**(1), 166–170.

59 S. Wurmehl, G. H. Fecher, H. C. Kandpal, V. Ksenofontov, C. Felser, H. J. Lin and J. Morais, Geometric, electronic, and magnetic structure of Co_2FeSi: Curie temperature and magnetic moment measurements and calculations, *Phys. Rev. B: Condens. Matter Mater. Phys.*, 2005, **72**(18), 184434.

60 S. Wurmehl, G. H. Fecher, H. C. Kandpal, V. Ksenofontov, C. Felser and H. J. Lin, Investigation of Co_2FeSi: The Heusler compound with highest Curie temperature and magnetic moment, *Appl. Phys. Lett.*, 2006, **88**(3), 032503.

61 T. Bandyopadhyay and D. D. Sarma, Calculation of Coulomb interaction strengths for 3d transition metals and actinides, *Phys. Rev. B: Condens. Matter Mater. Phys.*, 1989, **39**(6), 3517.

62 C. Herring, *Magnetism*, Academic Press, New York and London, 1966, vol. IV, p. 228.

63 B. N. Cox, M. A. Coulthard and P. Lloyd, A calculation of the Coulomb correlation energy, *U*, for transition metals in Hubbard's model, *J. Phys. F: Met. Phys.*, 1974, **4**(6), 807.

64 D. Do, M. S. Lee and S. D. Mahanti, Effect of onsite Coulomb repulsion on thermoelectric properties of full-Heusler compounds with pseudogaps, *Phys. Rev. B: Condens. Matter Mater. Phys.*, 2011, **84**(12), 125104.

65 S. Yousuf and D. C. Gupta, Insight into electronic, mechanical and transport properties of quaternary CoVTiAl: spin-polarized DFT+*U* approach, *J. Mater. Sci. Eng. B*, 2017, **221**, 73–79.

66 A. H. Reshak, Transport properties of Co-based Heusler compounds Co_2VAl and Co_2VGa: spin-polarized DFT+*U*, *RSC Adv.*, 2016, **6**(59), 54001–54012.

67 D. P. Rai, A. Shankar, M. P. Ghimire and R. K. Thapa, A comparative study of a Heusler alloy Co_2FeGe using LSDA and LSDA+*U*, *Phys. B*, 2012, **407**(18), 3689–3693.

68 D. P. Rai and R. K. Thapa, An abinitio study of the half-metallic properties of Co_2TGe (T= Sc, Ti, V, Cr, Mn, Fe): LSDA+*U* method, *J. Korean Phys. Soc.*, 2013, **62**(11), 1652–1660.

69 P. Giannozzi, S. Baroni, N. Bonini, M. Calandra, R. Car, C. Cavazzoni and A. Dal Corso, QUANTUM ESPRESSO: a modular and open-source software project for quantum simulations of materials, *J. Phys.: Condens. Matter*, 2009, **21**(39), 395502.

70 P. Blaha, K. Schwarz, G. K. Madsen, D. Kvasnicka and J. Luitz, *wien2k. An augmented plane wave+ local orbitals program for calculating crystal properties*, 2017.

71 H. J. Monkhorst and J. D. Pack, Special points for Brillouin-zone integrations, *Phys. Rev. B: Solid State*, 1976, **13**(12), 5188.

72 J. P. Perdew, K. Burke and M. Ernzerhof, Generalized gradient approximation made simple, *Phys. Rev. Lett.*, 1996, **77**(18), 3865.

73 M. Lazzeri, C. Attaccalite, L. Wirtz and F. Mauri, Impact of the electron-electron correlation on phonon dispersion: Failure of LDA and GGA DFT functionals in graphene and graphite, *Phys. Rev. B: Condens. Matter Mater. Phys.*, 2008, **78**(8), 081406.

74 N. Zaki, H. Park, R. M. Osgood, A. J. Millis and C. A. Marianetti, Failure of DFT-based computations for a stepped-substrate-supported correlated Co wire, *Phys. Rev. B: Condens. Matter Mater. Phys.*, 2014, **89**(20), 205427.

75 B. Barbiellini, E. G. Moroni and T. Jarlborg, Effects of gradient corrections on electronic structure in metals, *J. Phys.: Condens. Matter*, 1990, **2**(37), 7597.

76 A. I. Liechtenstein, V. I. Anisimov and J. Zaanen, Density-functional theory and strong interactions: Orbital ordering in Mott-Hubbard insulators, *Phys. Rev. B: Condens. Matter Mater. Phys.*, 1995, **52**(8), R5467.

77 O. Gunnarsson, O. K. Andersen, O. Jepsen and J. Zaanen, Density-functional calculation of the parameters in the Anderson model: Application to Mn in CdTe, *Phys. Rev. B: Condens. Matter Mater. Phys.*, 1989, **39**(3), 1708.

78 J. Van Den Brink, M. B. J. Meinders and G. A. Sawatzky, Influence of screening effects and inter-site Coulomb repulsion on the insulating correlation gap, *Phys. B*, 1995, **206**, 682–684.

79 S. Galehgirian and F. Ahmadian, First principles study on half-metallic properties of Heusler compounds Ti_2VZ (Z = Al, Ga, and In), *Solid State Commun.*, 2015, **202**, 52–57.

80 H. Luo, Y. Xin, B. Liu, F. Meng, H. Liu, E. Liu and G. Wu, Competition of $L2_1$ and XA structural ordering in Heusler alloys X_2CuAl (X = Sc, Ti, V, Cr, Mn, Fe, Co, Ni), *J. Alloys Compd.*, 2016, **665**, 180–185.

81 D. Bensaid, T. Hellal, M. Ameri, Y. Azzaz, B. Doumi, Y. Al-Douri and F. Benzoudji, First-principle investigation of structural, electronic and magnetic properties in Mn_2RhZ(Z= Si, Ge, and Sn) Heusler alloys, *J. Supercond. Novel Magn.*, 2016, **29**(7), 1843–1850.

82 V. K. Jain, N. Lakshmi, R. Jain and A. R. Chandra, Electronic Structure, Elastic, Magnetic, and Optical Properties of Fe_2MnZ (Z = Si, Ge, and Sn) Full Heusler Alloys: First-Principle Calculations, *J. Supercond. Novel Magn.*, 2019, **32**(3), 739–749.

83 H. Joshi, D. P. Rai, L. Hnamte, A. Laref and R. K. Thapa, A theoretical analysis of elastic and optical properties of half Heusler MCoSb (M= Ti, Zr and Hf), *Heliyon*, 2019, **5**(3), e01155.

84 S. C. Wu, S. S. Naghavi, G. H. Fecher and C. Felser, A critical study of the elastic properties and stability of Heusler compounds: Phase change and tetragonal X_2YZ compounds, *J. Mod. Phys.*, 2018, **09**(04), 83535.

85 M. Born and K. Huang, *Dynamical theory of crystal lattices*, Clarendon press, 1954.

86 L. Zuo, M. Humbert and C. Esling, Elastic properties of polycrystals in the Voigt-Reuss-Hill approximation, *J. Appl. Crystallogr.*, 1992, **25**(6), 751–755.

87 A. Abada, K. Amara, S. Hiadsi and B. Amrani, First principles study of a new half-metallic ferrimagnets Mn_2-based full Heusler compounds: Mn_2ZrSi and Mn_2ZrGe, *J. Magn. Magn. Mater.*, 2015, **388**, 59–67.

88 I. N. Frantsevich, F. F. Voronov and S. A. Bakuta, *Elastic Constants and Elastic Moduli of Metals and Nonmetals*, Naukova Dnmka, Kiev, 1982.

89 H. Zenasni, H. I. Faraoun and C. Esling, First-principle prediction of half-metallic ferrimagnetism in Mn-based full-Heusler alloys with highly ordered structure, *J. Magn. Magn. Mater.*, 2013, **333**, 162–168.

90 S. Ishida, S. Fujii, S. Kashiwagi and S. Asano, Search for half-metallic compounds in Co_2MnZ (Z= IIIb, IVb, Vb element), *J. Phys. Soc. Jpn.*, 1995, **64**(6), 2152–2157.

91 I. Galanakis, K. Özdoğan, E. Şaşıoğlu and B. Aktaş, Doping of Mn $_2$VAl and Mn_2VSi Heusler alloys as a route to half-metallic antiferromagnetism, *Phys. Rev. B: Condens. Matter Mater. Phys.*, 2007, **75**(9), 092407.

92 I. Galanakis, P. H. Dederichs and N. Papanikolaou, Slater-Pauling behavior and origin of the half-metallicity of the full-Heusler alloys, *Phys. Rev. B: Condens. Matter Mater. Phys.*, 2002, **66**(17), 174429.

